

High-temperature structural transformations in the relaxor ferroelectrics $\text{PbSc}_{0.5}\text{Ta}_{0.5}\text{O}_3$ and $\text{Pb}_{0.78}\text{Ba}_{0.22}\text{Sc}_{0.5}\text{Ta}_{0.5}\text{O}_3$

B. Mihailova,¹ B. Maier,¹ C. Paulmann,¹ T. Malcherek,¹ J. Ihringer,² M. Gospodinov,³ R. Stosch,⁴ B. Güttler,⁴ and U. Bismayer¹

¹*Mineralogisch-Petrographisches Institut, Universität Hamburg, Grindelallee 48, D-20146 Hamburg, Germany*

²*Institut für Angewandte Physik, Universität Tübingen, Auf der Morgenstelle 10, 72076 Tübingen, Germany*

³*Institute of Solid State Physics, Bulgarian Academy of Sciences, Boulevard Tzarigradsko Chausse 72, 1784 Sofia, Bulgaria*

⁴*Physikalisch-Technische Bundesanstalt, Bundesallee 100, 38116 Braunschweig, Germany*

(Received 28 November 2007; revised manuscript received 1 April 2008; published 8 May 2008)

Temperature-driven structural transformations in Pb-based perovskite-type relaxors are studied by using polarized Raman spectroscopy, high-resolution powder, and synchrotron single-crystal x-ray diffraction applied to $\text{PbSc}_{0.5}\text{Ta}_{0.5}\text{O}_3$ (PST) and $\text{Pb}_{0.78}\text{Ba}_{0.22}\text{Sc}_{0.5}\text{Ta}_{0.5}\text{O}_3$ (PBST). The two compounds were chosen as model systems because PST is a relaxor that exhibits ferroelectric long-range order on cooling, whereas PBST shows canonical relaxor behavior. The temperature evolution of phonon anomalies and the pseudocubic unit-cell parameter for both PST and PBST reveals the existence of a characteristic temperature T^* between the Burns temperature T_B and the temperature of the dielectric-permittivity maximum T_m . T^* is associated with the coupling of initially nucleated small polar clusters and their aggregation into larger polar clusters. The temperature range between T_B and T^* is characterized by a coupling between adjacent off-centered BO_6 octahedra to form initial polar clusters, while the range between T^* and T_m is characterized by a coupling between off-centered B cations from adjacent polar clusters. Off-centered Pb atoms exist even above the Burns temperature and their length of coherence governs the coupling between polar regions comprising B -cation off-center shifts and, consequently, directs the formation of the ferroelectric state to a normal, long-range ordered or nonergodic relaxor state.

DOI: [10.1103/PhysRevB.77.174106](https://doi.org/10.1103/PhysRevB.77.174106)

PACS number(s): 77.84.Dy, 64.70.Nd, 63.20.-e, 61.72.Dd

I. INTRODUCTION

Relaxor ferroelectrics are an important class of multifunctional materials with a wide range of applications including memory devices.^{1,2} The extremely high dielectric permittivity, strong electroelastic, and electro-optic coefficients of relaxors are related to their structural complexity.³ Relaxors differ from normal ferroelectrics in (i) the occurrence of a diffuse phase transition over a temperature range near the temperature of the dielectric-permittivity maximum T_m instead of an abrupt ferroic transition at the Curie temperature T_c and (ii) strong frequency dispersion of the dielectric permittivity as a function of temperature. Upon cooling, relaxors undergo a sequence of structural transformations. The first specific point is the so-called Burns temperature T_B characterized by the deviation of the refractive index from the linear dependence typical of the paraelectric state.⁴ At the Burns temperature, nucleation of dynamical polar nanoclusters occurs. The system is in the so-called ergodic (violated paraelectric) state consisting of dynamic, randomly oriented polar nanoclusters distributed within a paraelectric matrix. In the vicinity of T_m , the lifetime of polar clusters is on the order of microseconds⁵ and at the freezing temperature T_f , which is just below T_m , the system undergoes a phase transition from the ergodic to a nonergodic, relaxor ferroelectric state consisting of static, coupled polar nanoclusters. On further cooling, some relaxors [e.g., $\text{PbSc}_{0.5}\text{Ta}_{0.5}\text{O}_3$ (PST)] undergo a phase transition to a normal ferroelectric state, i.e., the formation of ferroelectric domains with well-developed ferroelectric long-range ordering (the correlation length of coherent atomic shifts from their positions in the paraelectric

phase is much longer than the unit-cell parameter), whereas canonical relaxors (e.g., $\text{PbMg}_{1/3}\text{Nb}_{2/3}\text{O}_3$) do not exhibit ferroelectric long-range ordering even at liquid-He temperatures. Recently, based on the temperature evolution of diffuse neutron and Raman scattering in $\text{PbMg}_{1/3}\text{Nb}_{2/3}\text{O}_3$ and $\text{PbZn}_{1/3}\text{Nb}_{2/3}\text{O}_3$, another characteristic temperature between T_B and T_f was proposed by Toulouse and co-workers.⁶⁻⁸ This temperature T^* was attributed to initial freezing of polar nanoclusters and hence, four main temperature ranges were assumed to be typical of relaxors: (i) a fully dynamic stage above T_B , (ii) quasidynamic behavior between T_B and T^* , (iii) quasistatic between T^* and T_f , and (iv) static below T_f . Besides, a change in the temperature dependence of the lowest-wave-number infrared-active mode at a temperature between T_f and T_B was observed for thin films of $\text{PbSc}_{0.5}\text{Ta}_{0.5}\text{O}_3$ and $\text{PbMg}_{1/3}\text{Nb}_{2/3}\text{O}_3$.^{9,10} Although the properties of thin films might deviate from those of bulk materials, these findings also indicated occurrence of atomic rearrangements at a certain temperature in the ergodic-state range. Acoustic-emission experiments on $\text{PbZn}_{1/3}\text{Nb}_{2/3}\text{O}_3$ and $(1-x)\text{PbZn}_{1/3}\text{Nb}_{2/3}\text{O}_3-x\text{PbTiO}_3$ confirmed the existence of an additional specific temperature above T_m and revealed that the corresponding structural transformations are associated with alteration in local elastic strains.^{11,12} The temperature of the observed acoustic activity for $\text{PbZn}_{1/3}\text{Nb}_{2/3}\text{O}_3$ is close to the temperature at which the cubic unit-cell constant deviates from the linear thermal-expansion behavior.^{12,13}

Thus, further structural studies on other relaxor compounds are required to verify the sequence of phase transformations at high temperatures and to better understand the atomistic mechanism of the formation and development of

polar nanoclusters. Hence, to give more insights on temperature-induced structural phenomena taking place in relaxors, we applied x-ray diffraction (XRD) and Raman spectroscopy to single crystals of $\text{PbSc}_{0.5}\text{Ta}_{0.5}\text{O}_3$ and $\text{Pb}_{0.78}\text{Ba}_{0.22}\text{Sc}_{0.5}\text{Ta}_{0.5}\text{O}_3$. We choose to study these two materials because $\text{PbSc}_{0.5}\text{Ta}_{0.5}\text{O}_3$ is a well-known relaxor that exhibits ferroelectric long-range ordering on cooling, while the recently synthesized compound $\text{Pb}_{0.78}\text{Ba}_{0.22}\text{Sc}_{0.5}\text{Ta}_{0.5}\text{O}_3$ (PBST) remains in the nonergodic, relaxor ferroelectric state well below T_m .¹⁴ The two experimental methods, x-ray diffraction and Raman scattering, have different length- and time-scale sensitivities, and their simultaneous application is very efficient to probe the local structural deviations (revealed by the anomalous Raman scattering) from the average structure as detected by diffraction techniques.

II. EXPERIMENT

Well-shaped cubiclike single crystals of $\text{PbSc}_{0.5}\text{Ta}_{0.5}\text{O}_3$ and $\text{Pb}_{0.78}\text{Ba}_{0.22}\text{Sc}_{0.5}\text{Ta}_{0.5}\text{O}_3$ of optical and chemical homogeneity were grown by the high-temperature solution growth method.^{14,15} Low-temperature powder XRD experiments were conducted between 20 and 300 K by using a homemade, high-resolution powder diffractometer operating in Guinier geometry¹⁶ and equipped with a Huber G670 image plate detector and a Cryophysics closed-cycle He cryostat. Data sets covered a 2θ range from 8° to 100° with a resolution of 0.005° and acquisition time of 30 min/pattern. High-temperature powder XRD measurements in the range of 300–1000 K were performed with a Philips X'Pert diffractometer (Bragg-Brentano geometry) by using an Anton Paar high-temperature cell. The XRD patterns were collected in a 2θ range from 15° to 84° , with a step size of 0.02° and an accumulation time of 4 s/step. Rietveld refinements were carried out by using the program SIMREF.¹⁷ Built-in temperature-dependent calibration of the 2θ scale on an internal silicon standard was applied for a precise determination of unit-cell parameters.

Synchrotron single-crystal XRD experiments were conducted at the F1 beamline of HASYLAB/DESY by using a high-energy radiation of wavelength $\lambda=0.4000 \text{ \AA}$ and a MarCCD 165 detector. Data were collected at a sample-to-detector distance of 50 mm with a step width of $1^\circ/\text{frame}$ with exposure times between 60 and 160 s. The experiments were performed at three different temperatures by using an in-house developed heating device and a liquid- N_2 cryostat (Oxford Cryosystems, Series 600).

Raman spectra were measured with a triple monochromator system Jobin-Yvon T64000 equipped with an Olympus BH2 microscope. The data were collected in backscattering geometry by using the 514.5 nm line of an Ar^+ laser and a beam power density on the sample surface of 2 kW/mm^2 . The Raman scattering was recorded at different temperatures in the range of 4–850 K, with a spectral resolution of 2 cm^{-1} . The low- and high-temperature data were collected by using a Cryovac cryogenic system and a LINKAM heating/cooling stage, respectively. In the temperature range of 100–290 K, spectroscopic measurements were performed with both devices to verify the reproducibility of the data.

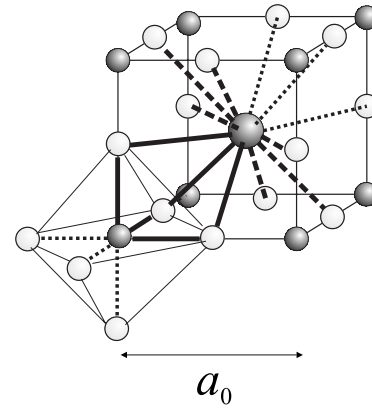


FIG. 1. Fragment of cubic perovskite-type structure; the large gray, small gray, and white circles represent A- and B-site cations and O, respectively. BO_3 -A atomic linkages along $\langle 111 \rangle$ and A-O layers perpendicular to $\langle 111 \rangle$ are underlined by presenting the corresponding bonds with bold solid and bold dashed lines. For the studied compounds, the B site is occupied by Sc and Ta, while the A site is occupied by Pb for PST and by Pb and Ba for PBST.

Polarized spectra in $Z(\text{XX})\bar{Z}$ and $Z(\text{XY})\bar{Z}$ scattering geometries (Porto notation) were collected at each temperature; X, Y, and Z are parallel to the cubic $\langle 100 \rangle$ crystallographic directions. The as-measured Raman spectra were subsequently reduced by the Bose-Einstein phonon occupation factor to eliminate the temperature dependence in the peak intensities. The peak positions, widths, and intensities were determined by fitting the temperature-reduced spectra with Lorentzian functions.

III. RESULTS AND DISCUSSION

PST and PBST are complex perovskite-type oxides of the general formula ABO_3 . The B-site cations are at the centers of oxygen octahedra, whereas A-site cations are at the centers of the cavities formed by eight BO_6 octahedra (Fig. 1). Coexistence of chemically B-site ordered and disordered regions is typical of relaxors.^{3,18} In the paraelectric state, the B-site disordered regions have a single-perovskite structure of $\text{Pm}\bar{3}\text{m}$ symmetry and a unit-cell parameter of $\sim 4 \text{ \AA}$, while the B-site ordered regions have a double-perovskite structure of $\text{Fm}\bar{3}\text{m}$ symmetry and a unit-cell parameter of $\sim 8 \text{ \AA}$. Both PST and PBST samples studied here exhibit B-site ordered domains detectable by powder XRD, and the average size of the B-site ordered spatial regions as determined from the full width at half maximum (FWHM) of the superlattice Bragg reflections is approximately 6 and 33 nm for PST and PBST, respectively.

Figure 2 shows representative (hkl) reciprocal-space sections of PST determined from the single-crystal synchrotron XRD data. The temperature evolution of the Bragg reflections and diffuse x-ray scattering reveals the phase transitions occurring upon cooling. From 700 to 300 K, when the system approaches $T_m \sim 280 \text{ K}$, strong diffuse scattering streaks along $\langle 110 \rangle$ develop. This diffuse scattering is typical of relaxors. It is associated with the intermediate-range struc-

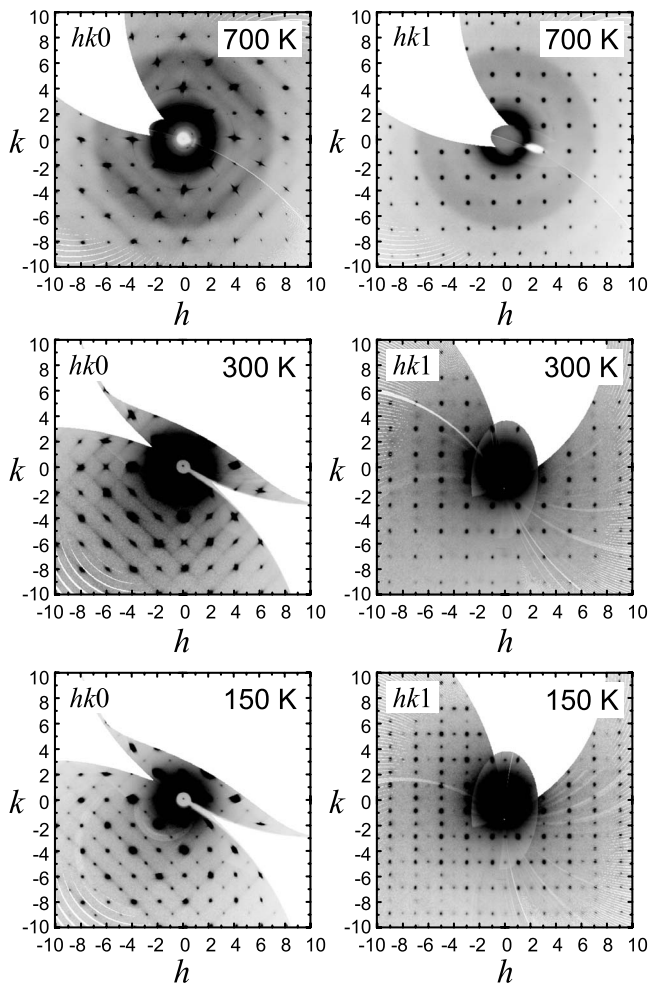


FIG. 2. $(hk0)$ and $(hk1)$ layers of the reciprocal space for $\text{PbSc}_{0.5}\text{Ta}_{0.5}\text{O}_3$ at three different temperatures; the Miller indices are given in a cubic double-perovskite $Fm\bar{3}m$ unit cell. The round features are artificial contributions from the quartz capillary.

tural ordering due to the existence of polar nanoclusters.^{19,20} The direction of diffuse scattering shows that the atomic ferroic shifts correlate within $\{110\}$ planes of the real space. However, the real-space direction of atomic deviations from the crystallographic positions of the cubic structure cannot unambiguously be determined from the observed diffuse scattering.²⁰ In particular, the preferred direction of Pb off-center shifts is rather controversial and all the three pseudocubic directions, $\langle 100 \rangle$, $\langle 110 \rangle$, and $\langle 111 \rangle$, have been proposed on the basis of different experimental methods.^{19–23} At $T=150$ K, which is below T_m , diffuse scattering for PST is strongly suppressed and additional Bragg reflections appear. The additional Bragg reflections seen at 150 K correspond to the crossings of the diffuse scattering streaks observed at 300 K [e.g., $(\bar{1}50)$] and reveal the occurrence of ferroelectric long-range ordering due to the enlarged correlation length between polar nanoclusters, i.e., the development of a normal ferroelectric state. The well-pronounced Bragg reflections in the $(hk1)$ layers indicate the presence of compositionally B -site ordered spatial regions in the structure.

The temperature dependence of the (hkl) layers for PBST is different from that of PST. As can be seen in Fig. 3, upon

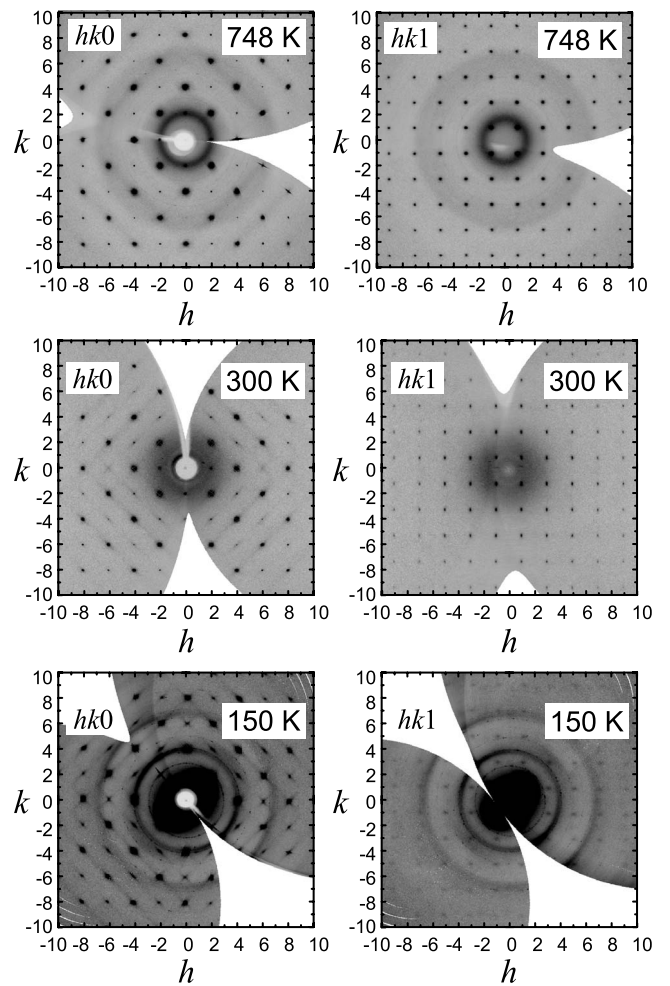


FIG. 3. $(hk0)$ and $(hk1)$ layers of the reciprocal space for $\text{Pb}_{0.78}\text{Ba}_{0.22}\text{Sc}_{0.5}\text{Ta}_{0.5}\text{O}_3$ at three different temperatures; the Miller indices are given in a cubic double-perovskite $(Fm\bar{3}m)$ unit cell. The round features are artificial contributions from the quartz capillary.

cooling, the diffuse scattering gradually increases in intensity and it is strongest at low temperatures. As an estimate, the ratio $I_{\text{DS}}/(I_{\text{BR}}+I_{\text{DS}})$ calculated for the $(\bar{8}40)$ point is approximately 0 at 748 K, 0.1×10^{-3} at 300 K, and 1.5×10^{-3} at 150 K; I_{BR} is the Bragg intensity determined from a fitted Voigt profile along the $[\bar{1}10]$ streak, while I_{DS} is the diffuse scattering determined as the difference between the average intensity of a parallel but off-peak profile and the baseline of the Bragg peak fitting. A similar tendency was found for other $(hk0)$ points with $h+k=4n$, i.e., with nominally additive scattering contributions from both A and B cations. No appearance of additional Bragg reflections due to a ferroic phase is observed at 150 K, which confirms the suppression of ferroelectric long-range ordering and the enhancement of a nonergodic, relaxor ferroelectric state as deduced from dielectric-permittivity experiments and polarized Raman spectroscopy.¹⁴ Interestingly, the Bragg reflections in the $(hk1)$ layer, which are related to chemically B -site ordered regions, become weaker and poorly resolved when the temperature decreases. Temperature lowering cannot induce hop-

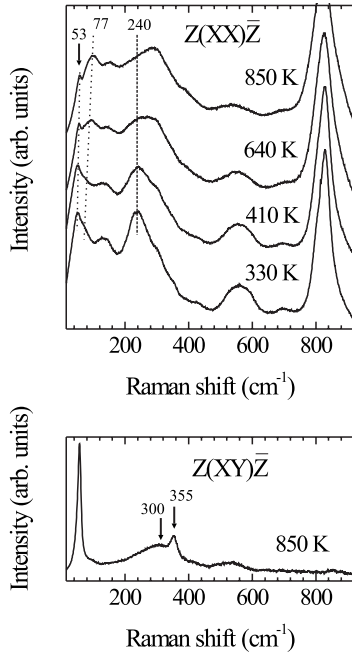


FIG. 4. Polarized Raman spectra of $\text{PbSc}_{0.5}\text{Ta}_{0.5}\text{O}_3$ collected at different temperatures above $T_m \sim 280$ K. The dotted lines in the upper plot indicate the anomalous Raman scattering near 53 and 77 cm^{-1} , which are related to the Pb-localized vibrations; the dashed line traces the position of the anomalous Raman scattering near 240 cm^{-1} which is related to the B -cation-localized mode. The arrows in the bottom plot mark the Raman scattering related to the Pb-O stretching mode.

ping of atoms from one B site to another and, therefore, a change in the chemical order cannot be expected on cooling. We assume that the observed phenomenon is due to the loss of periodicity in the B -cation system that results from a massive formation of very small-sized spatial regions comprising B -cation off-center shifts, i.e., polar nanoclusters. Because of the small coherence length of correlated B -cation off-center displacements, those spatial regions contribute much more strongly to the diffuse scattering in the $(hk0)$ layer rather than to the Bragg reflections in the $(hk1)$ layer. Hence, the existence of B -cation off-center displacements obstructs the observation of chemically B -site ordered regions. Another point that should be mentioned here is the strong weakening of the reflections stemming from $\{h00\}$ planes, where $h=6$. At $T=748$ K, neither the corresponding Bragg signal nor diffuse scattering is observed, at $T=300$ K, only a weak diffuse scattering along the $\langle 110 \rangle$ directions exists, whereas at $T=150$ K, a Bragg spot with the typical butterfly-shaped diffuse scattering appears. A similar suppression is observed for signals stemming from $\{hh2\}$ planes, where $h=4$ (not shown). The observed changes in the intensities are most probably due to Ba-doping-induced changes in the medium-range ordering of the Pb system.

Further information on the preferred atomic arrangements at high temperatures can be gained from Raman scattering. Figures 4 and 5 show polarized Raman spectra of PST and PBST, respectively, at temperatures above T_m . According to group theory, the Γ -point optical phonon modes of single-perovskite $Pm\bar{3}m$ cubic structure are $3F_{1u}(\text{IR})$

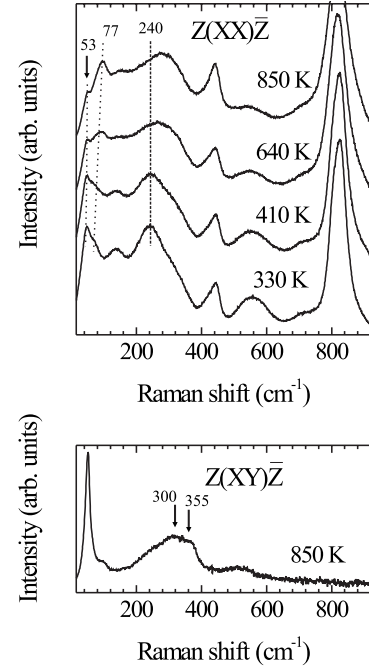


FIG. 5. Polarized Raman spectra of $\text{Pb}_{0.78}\text{Ba}_{0.22}\text{Sc}_{0.5}\text{Ta}_{0.5}\text{O}_3$ collected at different temperatures above $T_m \sim 200$ K. The dotted lines in the upper plot indicate the anomalous Raman scattering near 53 and 77 cm^{-1} , which are related to the Pb-localized vibrations; the dashed line traces the position of the anomalous Raman scattering near 240 cm^{-1} , which are related to the B -cation-localized mode. The arrows in the bottom plot mark the Raman scattering related to the Pb-O stretching mode.

$+F_{2u}(\text{inactive})$; none of them are Raman active. These phonon modes transform into $3A_1(\text{R, IR})+A_2(\text{inactive})+4E(\text{R, IR})$ when the system undergoes a paraelectric-to-ferroelectric $Pm\bar{3}m$ -to- $R3m$ phase transition. The Γ -point optical phonon modes of double-perovskite $Fm\bar{3}m$ cubic structure are $A_{1g}(\text{R})+E_g(\text{R})+4F_{1u}(\text{IR})+F_{1g}(\text{inactive})+F_{2u}(\text{inactive})+2F_{2g}(\text{R})$; the A_{1g} and E_g modes give rise to two peaks in the $Z(\text{XX})\bar{Z}$ polarized Raman spectrum, while the F_{2g} modes give rise to two peaks in the $Z(\text{XY})\bar{Z}$ polarized Raman spectrum. Under the paraelectric-to-ferroelectric phase transition, the cubic $Fm\bar{3}m$ modes transform into nine nondegenerate A modes and nine doubly degenerate E modes, which in $R3$ structure are all Raman active. More detailed site-symmetry analysis of phonon modes is given in Ref. 24.

So far, the Raman peaks observed at $T > T_m$ have been controversially ascribed to different cubic modes.^{25–28} However, it is a common opinion that (i) the Raman spectra of Pb-based relaxors are best interpreted in terms of double-perovskite prototype cubic structure, regardless of the degree of compositional B -site order determined by diffraction methods, (ii) the strong peak near 830 cm^{-1} originates from the A_{1g} mode related to the symmetrical stretching of BO_6 octahedra, and (iii) the Raman scattering near 53 cm^{-1} results from the Pb-localized F_{2g} mode. By considering the polarized Raman and synchrotron-based far-IR ellipsometric spectra of stoichiometric as well as A - and B -site-doped

$\text{PbSc}_{0.5}\text{Ta}_{0.5}\text{O}_3$ (PST) and $\text{PbSc}_{0.5}\text{Nb}_{0.5}\text{O}_3$ (PSN) single crystals, we were able to assign the observed Raman signals for these compounds to definite atomic vibrations.^{24,29–31} The origin of the Raman scattering near 240 cm^{-1} should be further discussed in detail, since it has been controversially related to cubic F_{2g} , F_{2u} , and F_{1u} modes. The strong B -cation-mass dependence of the Raman peak position observed for PST and PSN single crystals²⁴ as well as for PST-PSN ceramics³² clearly shows that the peak arises from a B -cation localized mode. The site-symmetry group analysis predicts a B -localized F_{1u} mode, which is IR active, and we indeed recorded the corresponding IR peaks for both PST and PSN.²⁹ The occurrence of deviations of B cations from their positions in the ideal perovskite structure would lead to Raman activity related to the B -localized F_{1u} mode of the cubic phase. Therefore, the Raman scattering near 240 cm^{-1} observed for Pb-based perovskite-type relaxors is due of cation off-center shifts in polar nanoregions. This assignment is in accordance with *ab initio* calculations on $\text{PbMg}_{1/3}\text{Nb}_{2/3}\text{O}_3$, which reveal the existence of a polar mode near 255 cm^{-1} involving Nb vibrations.³³

As can be seen in Figs. 4 and 5, for both PST and PBST, the $Z(\text{XX})\bar{Z}$ Raman signals that at room temperature appear near 53 and 77 cm^{-1} are observed also at $T=850\text{ K}$, which is above the typical values of T_B .⁴ Those signals arise from Pb-localized modes of ferroic species, which stem from the splitting of the Pb-localized F_{2g} mode of the cubic structure (the mode localization is determined from the type of atoms with the largest amplitude of vibration). Contribution of the Pb-localized mode of the paraelectric matrix to the $Z(\text{XX})\bar{Z}$ Raman scattering is symmetry forbidden. Thus, the existence of anomalous $Z(\text{XX})\bar{Z}$ Raman peaks near 53 and 77 cm^{-1} undoubtedly reveals the presence of Pb off-center shifts even at $T > T_B$. Our observations are in accordance with the results obtained from pair-distribution-function analysis.²³ Both peaks near 53 and 77 cm^{-1} soften with the temperature decrease, thus indicating that the corresponding phonon modes are involved in the structural transformations occurring on cooling. Another similarity between PST and PBST is the suppression of the peak near 240 cm^{-1} at $T=850\text{ K}$ and its strong enhancement on cooling. As explained above, this peak arises from the infrared-active F_{1u} mode localized in the B -site cations and its appearance in the Raman spectra is indicative for off-center shifts of B cations. Hence, the temperature evolution of Raman scattering at 240 cm^{-1} is related to the nucleation and development of polar clusters comprising B -cation off-center shifts. Another point that should be mentioned is the difference between PST and PBST in the intensity ratio of the Raman scattering at 300 and 355 cm^{-1} (see the bottom plots in Figs. 4 and 5). The anomalous Raman scattering near $300\text{--}350\text{ cm}^{-1}$ is related to the silent F_{2u} mode and involves Pb-O bond stretching vibrations within the Pb-O sheets parallel to $\{111\}$; the intensity ratio $\rho = I(355)/I(300)$ is indicative for the correlation length of coherent structural distortions in the Pb-O system.²⁴ Besides, the intensity ratio ρ measured at temperatures higher than T_m correlates with the depolarization of the Raman scattering observed at temperatures below T_m .^{30,31} The Raman-scattering depolarization related to the occur-

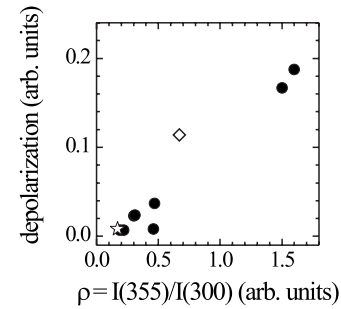


FIG. 6. Depolarization of Raman spectra measured at 4 K versus intensity ratio $\rho = I(355)/I(300)$ measured at 298 K in $Z(\text{XY})\bar{Z}$ scattering geometry for various lead scandium tantalate compounds: stoichiometric, Nb-, Sn-, Ba-, La-, and PST with different degrees of oxygen deficiency. For clarity, PST and PBST considered in this paper are given by an open diamond and star, respectively; the rest of the samples are given by black solid circles.

rence of ferroelectric long-range ordered domains below T_m was quantified via the intensity ratio $I_{cp}/(I_{pp}+I_{cp})$, where I_{cp} and I_{pp} denote the integrated intensity of the Raman-scattering band between 750 and 950 cm^{-1} measured in $Z(\text{XY})\bar{Z}$ and $Z(\text{XX})\bar{Z}$ geometries, respectively.³¹ As an example, Fig. 6 displays the depolarization of the spectra at 4 K versus the ratio ρ measured at 298 K for stoichiometric, Ba-, La-, Nb-, and Sn-doped PST as well as PST with enhanced and suppressed oxygen deficiency.^{30,31} The trend between $I_{cp}/(I_{pp}+I_{cp})$ and ρ shows that larger correlation between distorted Pb-O species leads to development of long-range ferroelectric ordering and vice versa.

Due to the dilution of the Pb system with Ba, the coherent length of distorted Pb-O species is shorter than that of PST, as revealed by the decrease in the intensity ratio ρ . Consequently, PBST exhibits no development of ferroelectric long-range ordering, as shown by the preserved polarization of the Raman spectra,¹⁴ the frequency dispersion of the dielectric permittivity,¹⁴ and the absence of additional Bragg reflections (Fig. 3) at low temperatures. Therefore, the high-temperature Raman data presented here show that the incipient ferroic Pb-O species exist even at temperatures above T_B and are an inherent structural feature related to the chemical composition.

It has been demonstrated that the temperature dependence of the position, width, and intensity of the lowest-wavenumber unpolarized Raman signal reflects the development of the ferroelectric state in PST.³⁴ Hence, to gain deeper insights into structural phenomena in relaxors, we considered the trends of the polarized Raman signals. Figure 7 displays the temperature dependence of the square wave number ω^2 of the allowed $[Z(\text{XY})\bar{Z}]$ and the anomalous $Z(\text{XX})\bar{Z}$ Raman scattering near 53 cm^{-1} , which is generated from the Pb-localized phonon mode. When the temperature is changed from 850 K to $T_m \sim 280\text{ K}$, the symmetry-allowed peak, which results from the cubic F_{2g} mode, linearly decreases in wave number, while the temperature dependence of the anomalous Raman scattering is more complex. Initially, the anomalous signal follows the trend of the allowed signal, but near 700 K , it deviates from the linear dependence and starts

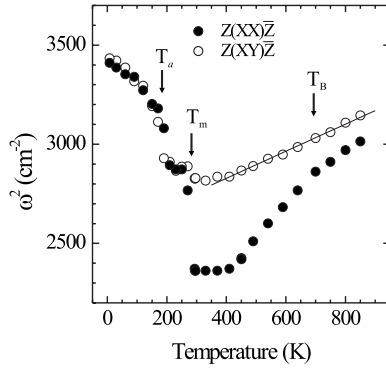


FIG. 7. Temperature dependence of the square wave number ω^2 of the allowed $Z(XY)\bar{Z}$ and anomalous $Z(XX)\bar{Z}$ Raman scatterings near 53 cm^{-1} measured for $\text{PbSc}_{0.5}\text{Ta}_{0.5}\text{O}_3$. The line represents the linear fit of $\omega^2(T)$ at $T > 400 \text{ K}$ for the allowed Raman scattering (F_{2g} mode in $Fm\bar{3}m$).

to more strongly soften, similarly to the deviation of the temperature dependence of the refractive index from the expected linear trend typical of paraelectrics.⁴ Thus, we propose that the temperature of deviation of $\omega^2(T)$ of the $Z(XX)\bar{Z}$ peak near 53 cm^{-1} from the $\omega^2(T)$ of the $Z(XY)\bar{Z}$ peak corresponds to the Burns temperature. Near 420 K , the anomalous peak stops softening and between 420 and 290 K , $\omega^2(T)$ has a plateaulike shape, thus indicating additional structural transformation processes between T_B and T_m . Below T_m , the temperature dependence of the peak positions observed in $Z(XX)\bar{Z}$ and $Z(XY)\bar{Z}$ spectra becomes the same because long-range ordered ferroelectric domains of rhombohedral symmetry are formed. Hence, the peaks originate from rhombohedral phonon modes and can no longer be considered in terms of “anomalous” and “allowed” signals coming from the cubic F_{2g} mode. Another kink in $\omega^2(T)$ is observed at $T_a \sim 190 \text{ K}$, which is related to lowering of the rotational local symmetry as revealed by the additional splitting of the Raman peaks.²⁹

The ferroelectricity in perovskite-type structures that have a transition metal element at the B site is related to off centering of the B -site cations.³⁵ If the A site is occupied by lead, the Pb off shifts are of vital importance for the occurrence of spontaneous polarization.^{23,36} However, electronic-structure calculations for the two classical ferroelectrics, BaTiO_3 and PbTiO_3 , demonstrated that in both perovskite materials, the hybridization between the $3d$ states of the B -positioned Ti ions and the $2p$ states of oxygen is essential for stabilizing the ferroelectric distortion.³⁶ In addition, the so-called Slater mode, comprising B -cation oscillations against the six octahedral oxygen atoms, is the strongest idealized mode of the simple perovskite structure even for Pb-based materials.³⁷ Thus, to better understand the formation of polar nanoclusters in relaxors, we have to carefully examine also the behavior of the anomalous Raman peak at 240 cm^{-1} , which arises from off-shifted B cations. Figure 8 shows the temperature dependence of ω^2 , FWHM, and the total intensity I of the Raman scattering near 240 cm^{-1} for PST. Below T_m , the peak first splits in two and then, at T_a , in three components due to the formation of the long-range

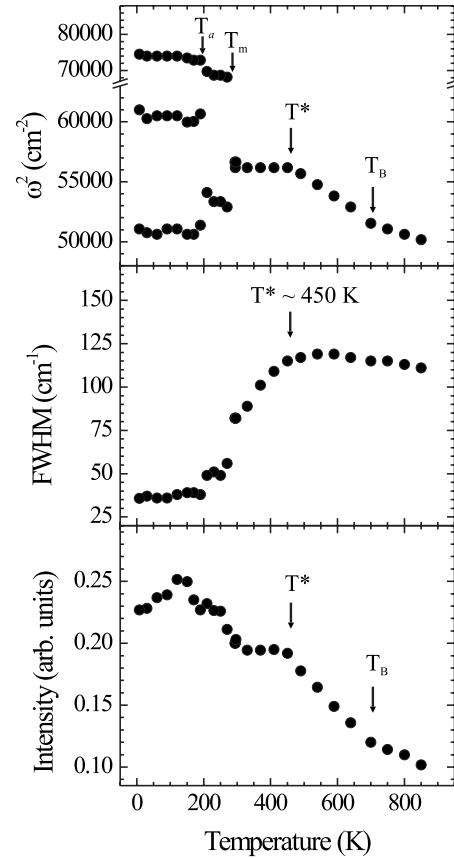


FIG. 8. Temperature dependence of the square wave number, FWHM for the most intense component, and total intensity of the Raman scattering near 240 cm^{-1} measured for $\text{PbSc}_{0.5}\text{Ta}_{0.5}\text{O}_3$ in $Z(XX)\bar{Z}$ scattering geometry.

ferroelectric state. The peak width at $T < T_m$ is plotted for the most intense component. It is worth noting that very weak and broad, poorly resolved Raman scattering is observed also at 850 K , which indicates occasional B -cation off-center fluctuations of dynamical character. The Burns temperature can also be deduced from the change in the slope of $\omega^2(T)$ and $I(T)$. At $T_B = 700 \text{ K}$, the instantaneous Ba-cation displacements couple and form small-sized spatial regions comprising off-centered BO_6 octahedra—initial small polar clusters. At $T < T_B$, the increase in wave number and intensity is stronger than that at $T > T_B$ due to the gradual increase in the off centering of the BO_6 octahedra and the number of such octahedra, i.e., due to nucleation and further growth of the polar clusters. At 450 K , the system reaches saturation: (i) no further change in wave number, which means no further increase in the B -cation off-centered shifts; and (ii) no further change in intensity, which means no further formation of off-centered O_6 octahedra, within the sensitivity of Raman spectroscopy. On the other hand, the huge decrease in FWHM between 450 K and T_m indicates strong correlation processes between already formed small polar clusters comprising off-centered B cations. Thus, we suggest that the strong drop of FWHM of the anomalous Raman scattering near 240 cm^{-1} defines best the temperature T^* —coupling of initial small polar clusters and their aggregation in larger polar clusters, i.e., initial freezing of polar nanoregions as

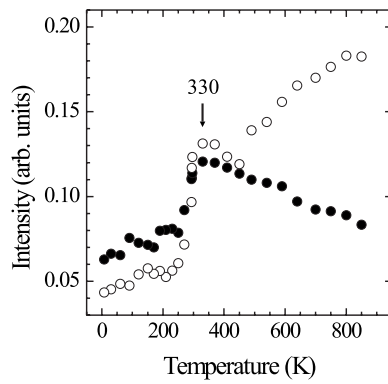


FIG. 9. Temperature dependence of the intensity of the Raman scattering near 135 cm^{-1} (filled circles) and between $300\text{ and }350\text{ cm}^{-1}$ (open circles), which is related to the BO_3 -Pb translational mode and Pb-O stretching mode, respectively, measured for $PbSc_{0.5}Ta_{0.5}O_3$ in $Z(XX)\bar{Z}$ scattering geometry.

proposed by Toulouse *et al.*⁸ In this sense, the temperature range between T_B and T^* can be considered as the range of intracluster structural phenomena, while the range between T^* and T_m as the range of intercluster structural phenomena. Hence, the development of the relaxor ferroelectric state is a two-step process: (i) coupling between off-center shifts of adjacent atoms to form incipient polar spatial regions embedded in a paraelectric matrix and (ii) coupling between off-center shifts of atoms from adjacent polar spatial regions to extend and join those regions at the expense of the paraelectric substance between them. One should mention that just below $T^* \sim 450\text{ K}$, the wave number of the anomalous Pb-localized mode near 53 cm^{-1} becomes a constant down to approximately $T_m \sim 280\text{ K}$ (see Fig. 7). The intensity and the FWHM of this peak (not shown) are also almost constant within the range $T^* - T_m$. This indicates structural saturation in the system of off-centered Pb atoms and implies that massive coupling of the off-centered Pb atoms takes place within near the same temperature range as that of the coupling between off-centered BO_6 octahedra from different polar regions. Therefore, for PST, strong intercluster interactions occur between T^* and T_m , thus leading to a formation of ferroelectric long-range ordering.

A challenging problem is to distinguish phonon modes involved in the intercluster coupling from the rest of the anomalous phonons. Such modes should substantially comprise vibrations of atoms at the interface between the polar spatial regions and the paraelectric matrix. For relaxors that exhibit ferroelectric long-range ordering, the number of interface atoms should initially increase because of the enlargement of the polar nanoclusters and then it should decrease due to merging of clusters in domains. Hence, the intensity of such modes should have a maximum within the temperature range of intercluster coupling. PST undergoes a phase transition to the normal ferroelectric state, which makes this compound a very suitable model system. The analysis of the temperature evolution of Raman scattering for PST reveals that two modes indeed show such a feature (see Fig. 9). The integrated intensity of the Raman scattering near 135 cm^{-1} , which is related to the infrared-active translation

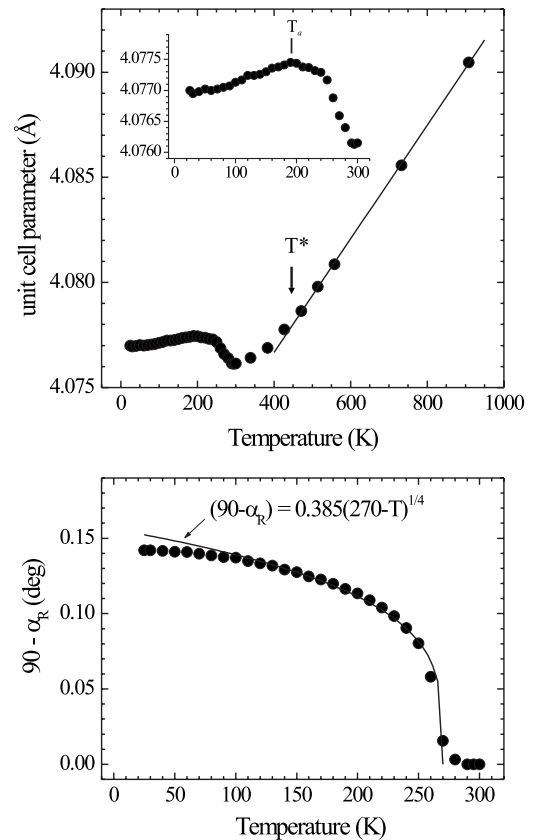


FIG. 10. Temperature dependence of the unit-cell parameters of $PbSc_{0.5}Ta_{0.5}O_3$ calculated in a single-perovskite structure. The line in the upper plot represents the linear fit of $a(T)$ at high temperatures, while the line in the bottom plot represents the power-function fit of the deviation of the unit-cell angle from 90° .

mode F_{1u} involving motions of BO_3 units against Pb atoms,²⁴ as well as the Raman scattering at $300\text{--}355\text{ cm}^{-1}$, which is related to the silent F_{2u} mode and comprises Pb-O bond stretching vibrations within the Pb-O sheets,²⁹ have a maximum near 330 K . The former mode consists of vibrations of all types of atoms (oxygen and A- and B-site cations), and it is reasonable to expect that this mode is involved in intercluster interactions. The more interesting fact is that the Pb-O stretching mode is also responsible for cluster coupling. This explains the observed correlation between the intensity ratio $\rho = I(355)/I(300)$ and the development of ferroelectric domains as discussed above. Furthermore, this emphasizes the fact that the incipient ferroic Pb-O species existing above T_B govern the coupling between spatial polar regions comprising off-centered B cations and, thus, direct the formation of the ferroelectric state.

To check whether the structural phenomena that take place near T^* affect the average structure, we performed powder XRD analysis at different temperatures. As can be seen in Fig. 10, the existence of a phase transition in the vicinity of $T^* \sim 450\text{ K}$ defined from the temperature evolution of the B-localized phonon anomaly is also revealed by the temperature dependence of the unit-cell constant. Below 450 K , the pseudocubic unit-cell constant clearly deviates from the linear dependence characteristic of high temperatures, thus revealing the occurrence of structural transforma-

tion. The change in the $a(T)$ gradient at T^* indicates a change in the thermal-expansion properties, which is most probably related to the occurrence of local elastic fields at the interface between the polar nanoclusters and the cubic matrix. Our low-temperature data are in good accordance with the structure refinement based on high-resolution neutron diffraction data.³⁸ A paraelectric-to-ferroelectric phase transition from the cubic $Fm\bar{3}m$ to the rhombohedral $R3$ structure occurs at 280 K. Since $R3$ is a polar crystal class, the deviation of the unit-cell angle α_R (rhombohedral setting) from 90° is related to spontaneous polarization and, hence, $90-\alpha_R$ can be used as an order parameter. As can be seen in Fig. 10, $90-\alpha_R$ follows the $A(T_c-T)^{1/4}$ dependence, as found by Woodward and Baba-Kishi,³⁸ who suggested that this result indicates a weak first-order phase transition approaching a tricritical point. It is worth noting that the rhombohedral unit-cell constant a has a maximum at $T=190$ K, which corresponds well to the temperature T_a , determined from the temperature dependence of the Raman spectra. The comparison between the temperature evolution of the unit-cell parameters and Raman scattering reveals that just below T_m , the parameter $90-\alpha_R$ becomes nonzero, thus indicating the occurrence of cubic-to-rhombohedral transition. Accordingly, below T_m , the Raman peaks originating from cubic F modes split into two components, corresponding to rhombohedral A and E modes. Between T_m and T_a , the unit-cell parameter a increases with the temperature decrease, whereas below T_a , $a(T)$ follows the ordinary trend. At the same time, below T_a , the Raman peaks originating from the cubic F modes further split to three components,^{29,30} which evidences additional lowering of the local symmetry. Indeed, Woodward and Baba-Kishi³⁸ refined the average structure of PST at 4.2 K by considering the coexistence of cation-oxygen polyhedra that have C_3 and C_1 symmetries. Therefore, the complementary XRD and Raman data presented here indicate that the development of long-range ferroelectric ordering in PST may be considered as a two-step process: (i) rhombohedral distortion of the unit cell just below T_m and (ii) atomic rearrangements that lower the local symmetry below T_a .

The temperature dependence of ω^2 of the allowed $Z(XY)\bar{Z}$ and anomalous $Z(XX)\bar{Z}$ signal near 53 cm^{-1} for PBST is presented in Fig. 11. Similarly to PST, T_B is well defined via the temperature at which $\omega^2(T)$ for the anomalous Raman scattering deviates from the linear trend of the allowed scattering. For both PST and PBST, T_B is found to be near 700 K. However, the overall behavior of the Pb-localized mode in PBST substantially differs from that of PST. Contrarily to PST, below T_m , the anomalous and the allowed scatterings near 53 cm^{-1} have different temperature dependences, which mirror the absence of long-range ferroelectric domains. The anomalous signal at 53 cm^{-1} exhibits a broad minimum at 350 K instead of a plateaulike $\omega^2(T)$ dependence, as in the case of PST. This implies that coupling processes within the system of off-centered Pb atoms are weaker in PBST as compared to those in PST. The latter is consequent from the partial substitution of Ba for Pb. Below 350 K, the allowed $Z(XY)\bar{Z}$ signal shows no hardening on cooling, which also indicates the absence of transition to normal ferroelectric state. The slight kink in $\omega^2(T)$ of the anomalous

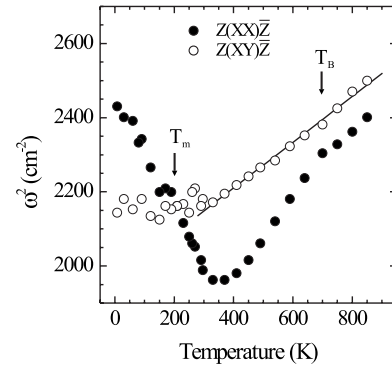


FIG. 11. Temperature dependence of the square wave number ω^2 of the allowed $Z(XY)\bar{Z}$ and anomalous $Z(XX)\bar{Z}$ Raman scattering near 53 cm^{-1} measured for $\text{Pb}_{0.78}\text{Ba}_{0.22}\text{Sc}_{0.5}\text{Ta}_{0.5}\text{O}_3$. The line represents the linear fit of $\omega^2(T)$ at $T > 400$ K for the allowed Raman scattering (F_{2g} mode in $Fm\bar{3}m$).

Pb-localized signal marks the temperature of the dielectric maximum T_m .

Figure 12 shows the temperature dependence of ω^2 , FWHM, and I of the Raman scattering near 240 cm^{-1} related to the B -localized F_{1u} mode for PBST. The temperature T^* is again well defined as the point where FWHM strongly

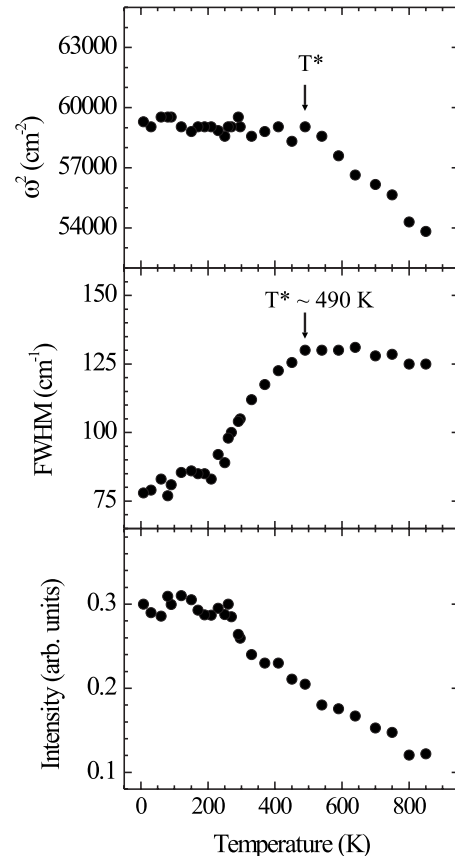


FIG. 12. Temperature dependence of the square wave number, FWHM, and total intensity of the Raman scattering near 240 cm^{-1} measured for $\text{Pb}_{0.78}\text{Ba}_{0.22}\text{Sc}_{0.5}\text{Ta}_{0.5}\text{O}_3$ in $Z(XX)\bar{Z}$ scattering geometry.

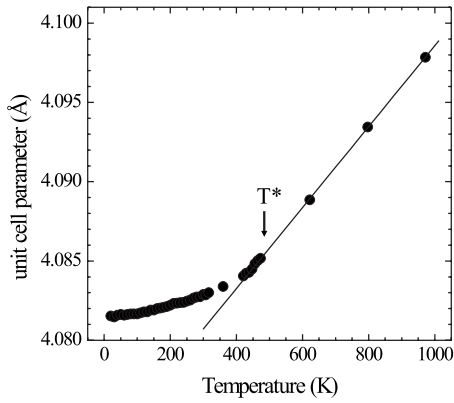


FIG. 13. Temperature dependence of the unit-cell constant of $\text{Pb}_{0.78}\text{Ba}_{0.22}\text{Sc}_{0.5}\text{Ta}_{0.5}\text{O}_3$ calculated in a single-perovskite structure. The line represents the linear fit of $a(T)$ at high temperatures.

decreases. For PBST, T^* is ~ 490 K. Below T^* , the square wave number is almost constant, which suggests saturation of local structural deformations, i.e., the maximum of BO_6 off centering is reached for the majority of the distorted species. However, the prominent increase in intensity at $T < T^*$ reveals that the intercluster coupling processes are accompanied by further occurrence of polar species comprising off-centered B cations. This observation is consistent with the canonical relaxor behavior of PBST, which shows frequency dispersion of the dielectric permittivity at low temperature.¹⁴ As expected, $I(T)$ becomes almost constant below T_m , which points to no or negligible further nucleation of polar clusters containing off-center shifts of B cations. For PBST, the coupling processes in the Pb system are smooth and not as well pronounced as in the case of PST. The square wave number of the anomalous Pb-localized mode near 53 cm^{-1} shows a broad minimum centered near 350 K , which is well below T^* , i.e., well below the temperature of massive coupling of off-centered B -site cations. Hence, weaker intercluster interactions occur for PBST between T^* and T_m , which are not strong enough to induce a formation of long-range ordered ferroelectric domains.

The temperature dependence of the pseudocubic unit-cell parameter a of PBST is shown in Fig. 13. The high-resolution powder x-ray diffraction data again confirm the absence of a ferroelectric phase transition below T_m . As in the case of PST, near T^* , a deviation of $a(T)$ from the linear trend is observed, which again underlines that T^* is a fundamental characteristic point of relaxors that exhibit a normal ferroelectric state and those remaining in a nonergodic state. It is worth noting that in perovskite-type structures, Ba and Pb cations have the same valence, i.e., no local electrical fields due to charge imbalance are induced upon Ba doping of PST. Therefore, the suppression of long-range ordering and the enhancement of nonergodic relaxor state is related to the occurrence of local structural distortions and consequent local elastic strains resulting from the difference in the ionic radii of Ba^{2+} and Pb^{2+} . The fact that the size of chemically B -site ordered domains is larger for PBST as compared to

PST also highlights the primary importance of local elastic strains for the formation of relaxor ferroelectric state in perovskite-type materials.

IV. CONCLUSIONS

Our results on PST and PBST confirm the existence of a fundamental characteristic temperature T^* , which is typical for relaxor ferroelectrics and occurs between T_m and T_B . It is demonstrated that T^* is associated with the coupling of polar clusters and their aggregation into larger clusters. The Burns temperature T_B at which polar clusters comprising B -cation off shifts nucleate as well as the temperature T^* at which initial cluster coupling occurs can be determined by using hard-mode polarized Raman spectroscopy.

The Burns temperature can be deduced from the deviation of $\omega^2(T)$ for the lowest-energy Raman signal observed in $Z(\text{XX})\bar{Z}$ scattering geometry from the linear trend typical of the lowest-energy symmetry-allowed Raman signal observed in $Z(\text{XY})\bar{Z}$ scattering geometry. The temperature T^* associated with the occurrence of polar-cluster coupling can be determined by the temperature at which the FWHM of the $Z(\text{XX})\bar{Z}$ Raman signal near 240 cm^{-1} , resulting from the B -cation-localized mode, strongly decreases. The range $T_B - T^*$ can be considered as the range of intracluster structural phenomena: coupling between off-center shifts of adjacent atoms to form incipient polar spatial regions embedded in a paraelectric matrix, whereas the range $T^* - T_m$ is the range of intercluster structural phenomena: coupling between off-center shifts of atoms from adjacent polar spatial regions to aggregate those regions on the account of the surrounding paraelectric substance.

Off-centered Pb atoms and thus incipient ferroic Pb-O structural species with a size and a lifetime large enough to be detected by Raman spectroscopy exist even above T_B . The length of coherence within the Pb-O system strongly influences the strength of coupling between spatial polar regions comprising off-centered B cations. A high degree of coherence between the Pb off-center shifts leads to strong interaction between polar clusters comprising B -cation off-center shifts and, consequently, to the development of long-range ordered ferroelectric domains. A low degree of coherence between the Pb off-center shifts leads to weak interaction between polar clusters comprising B -cation off-center shifts and, consequently, to suppression of ferroelectric long-range ordering.

ACKNOWLEDGMENTS

Financial support by Deutsche Forschungsgemeinschaft (Grants No. MI 1127/1-1 and No. MI 1127/1-2) and the Bulgarian Ministry of Science and Education (Grants No. NT 1-02 and No. BYX 308) is acknowledged. The authors are grateful to Ross Angel, Virginia Tech, and Ekhard Salje, University of Cambridge, for valuable and fruitful discussions and thank Joachim Ludwig, University of Hamburg, for collecting the powder XRD data at high temperatures.

- ¹A. S. Bhalla, R. Guo, and R. Roy, *Mater. Res. Innovations* **4**, 3 (2000).
- ²J. F. Scott, *J. Phys.: Condens. Matter* **18**, R361 (2006).
- ³A. A. Bokov and Z.-G. Ye, *J. Mater. Sci.* **41**, 31 (2006).
- ⁴G. Burns and B. A. Scott, *Solid State Commun.* **13**, 423 (1973).
- ⁵R. Blinc, A. Gregorovic, B. Zalar, R. Pirc, V. V. Laguta, and M. D. Glinchuk, *Phys. Rev. B* **63**, 024104 (2000).
- ⁶D. La-Orautapong, J. Toulouse, J. L. Robertson, and Z.-G. Ye, *Phys. Rev. B* **64**, 212101 (2001).
- ⁷O. Svitelskiy, J. Toulouse, G. Yong, and Z.-G. Ye, *Phys. Rev. B* **68**, 104107 (2003).
- ⁸J. Toulouse, F. Jiang, O. Svitelskiy, W. Chen, and Z.-G. Ye, *Phys. Rev. B* **72**, 184106 (2005).
- ⁹S. Kamba, M. Berta, M. Kempa, J. Hlinka, J. Petzelt, K. Brinkman, and N. Setter, *J. Appl. Phys.* **98**, 074103 (2005).
- ¹⁰S. Kamba, M. Kempa, V. Bovtun, J. Petzelt, K. Brinkman, and N. Setter, *J. Phys.: Condens. Matter* **17**, 3965 (2005).
- ¹¹E. Dul'kin, M. Roth, P. E. Janolin, and B. Dkhil, *Phys. Rev. B* **73**, 012102 (2006).
- ¹²M. Roth, E. Mojaev, E. Dulkan, P. Gemeiner, and B. Dkhil, *Phys. Rev. Lett.* **98**, 265701 (2007).
- ¹³T. Iwase, H. Tazana, K. Fujishiro, Y. Uesu, and Y. Yamada, *J. Phys. Chem. Solids* **60**, 1419 (1999).
- ¹⁴V. Marinova, B. Mihailova, T. Malcherek, C. Paulmann, K. Lengyel, L. Kovacs, M. Veleva, M. Gospodinov, B. Güttler, R. Stosch, and U. Bismayer, *J. Phys.: Condens. Matter* **18**, L385 (2006).
- ¹⁵V. Marinova, D. Petrova, M. Gospodinov, and S. Dobрева, *Mater. Res. Bull.* **32**, 663 (1997).
- ¹⁶J. Ihringer, *J. Appl. Crystallogr.* **15**, 1 (1982).
- ¹⁷J. K. Maichle, J. Ihringer, and W. Prandl, *J. Appl. Crystallogr.* **21**, 22 (1988).
- ¹⁸M. P. Harmer, J. Chen, P. Peng, H. M. Chan, and D. M. Smyth, *Ferroelectrics* **97**, 263 (1989).
- ¹⁹T. R. Welberry, D. J. Goossens, and M. J. Gutmann, *Phys. Rev. B* **74**, 224108 (2006).
- ²⁰M. Pasciak, M. Wolczyk, and A. Pietraszko, *Phys. Rev. B* **76**, 014117 (2007).
- ²¹I.-K. Jeong and J. K. Lee, *Appl. Phys. Lett.* **88**, 262905 (2006).
- ²²R. Blinc, V. Laguta, and B. Zalar, *Phys. Rev. Lett.* **91**, 247601 (2003).
- ²³T. Egami, *Annu. Rev. Mater. Res.* **37**, 297 (2007).
- ²⁴B. Mihailova, U. Bismayer, B. Güttler, M. Gospodinov, and L. Konstantinov, *J. Phys.: Condens. Matter* **14**, 1091 (2002).
- ²⁵I. G. Siny, R. S. Katiyar, and A. S. Bhalla, *Ferroelectr. Rev.* **2**, 51 (2000).
- ²⁶F. Jiang, S. Kojima, C. Zhao, and C. Feng, *Appl. Phys. Lett.* **79**, 3938 (2001).
- ²⁷J. Kreisel, B. Dkhil, P. Bouvier, and J.-M. Kiat, *Phys. Rev. B* **65**, 172101 (2002).
- ²⁸B. Hehlen, G. Simon, and J. Hlinka, *Phys. Rev. B* **75**, 052104 (2007).
- ²⁹B. Mihailova, U. Bismayer, B. Güttler, M. Gospodinov, A. Boris, C. Bernhard, and M. Aroyo, *Z. Kristallogr.* **220**, 740 (2005).
- ³⁰B. Mihailova, M. Gospodinov, B. Güttler, D. Petrova, R. Stosch, and U. Bismayer, *J. Phys.: Condens. Matter* **19**, 246220 (2007).
- ³¹B. Mihailova, M. Gospodinov, B. Güttler, R. Stosch, and U. Bismayer, *J. Phys.: Condens. Matter* **19**, 27520 (2007).
- ³²M. Correa, R. G. Choudhary, and R. S. Katiyar, *J. Appl. Phys.* **101**, 054116 (2007).
- ³³N. Choudhury, Z. Wu, E. J. Walter, and R. E. Cohen, *Phys. Rev. B* **71**, 125134 (2005).
- ³⁴U. Bismayer, V. Devarajan, and E. Salje, *J. Phys.: Condens. Matter* **1**, 6977 (1989).
- ³⁵N. A. Hill, *J. Phys. Chem. B* **104**, 6694 (2000).
- ³⁶R. E. Cohen, *Nature (London)* **358**, 136 (1992).
- ³⁷J. Hlinka, J. Petzelt, S. Kamba, D. Noujni, and T. Ostapchuk, *Phase Transitions* **79**, 41 (2006).
- ³⁸P. M. Woodward and K. Z. Baba-Kishi, *J. Appl. Crystallogr.* **35**, 233 (2002).